Generating and measuring non-diffracting vector Bessel beams

A. Dudley[*a], Y. Li[b], T. Mhlanga[a], M. Escuti[b] and A. Forbes[a].
[a]CSIR National Laser Centre, P.O. Box 395, Pretoria 0001, South Africa.
[b]Department of Electrical and Computer Engineering, North Carolina State University, Rayleigh, North Carolina 27695, USA.

ABSTRACT

We demonstrate how to create non-diffracting vector Bessel beams by implementing a spatial light modulator (SLM) to generate scalar Bessel beams which are then converted into vector fields by the use of an azimuthally-varying birefringent plate, known as a q-plate. The orbital angular momentum (OAM) of these generated beams is measured by performing a modal decomposition on each of the beam's polarization components. This is achieved by separating the circular polarization components through a polarization grating (PG) before performing the modal decomposition. We investigate both single charged Bessel beams as well as superpositions and the results are in good agreement with theory.

Keywords: vector fields, Bessel beams, orbital angular momentum.

1. INTRODUCTION

Polarization is a fundamental and well-studied property of light. Most investigations assume optical modes of spatially homogeneous polarization (such as linear, circular and elliptical), however studies into unconventional or spatially inhomogeneous polarization states are becoming more popular. Modes with spatially varying polarization states can be classified as having a cylindrical symmetric polarization, commonly referred to as cylindrical vector (CV) beams [1], which consist of radial, azimuthal and a linear superposition of the two to form generalized cylindrical polarization.

Developments in CV beams have been reviewed in numerous publications [1-4]. In the cross-sectional profile of these CV beams, the local polarization state is linearly polarized at different orientations, resulting in them occupying the equator on the Poincare Sphere. However, a more general type of vector beam (Full Poincare (FP) beams), whose local polarization state spans the entire surface of the Poincare sphere, has recently been proposed [5]. Various methods of generating vector beams have been developed from laser gain media [6, 7], optical fibres [8], radial polarization converters (such as q-plates) and liquid crystal displays [9, 10]. The unique properties of CV beams such as tight focusing under high numerical-aperture focusing has given rise to many applications ranging from spectroscopy [11], and particle manipulation [12]. These beams have also been shown to be more resilient to atmospheric turbulence [13] proving useful in remote sensing and free space optical communication.

This concept of spatially inhomogeneous polarization can be combined with a scalar vortex field that has a helical phase structure around a singular point [14], to produce vector vortex beams [15-19]. These scalar vortex fields which carry orbital angular momentum (OAM) have an azimuthal angular dependence of $\exp(il\theta)$ [20, 21] where l is the azimuthal index and θ is the azimuthal angle. Propagation-invariant scalar modes which are OAM-carriers are higher-order Bessel beams [22-25]. These modes have found applications in optical tweezing [26] and quantum optics [27] due to their invariant nature and their ability to reconstruct after encountering an obstacle [28-30]. Experimental studies into non-diffracting vector beams have remained somewhat limited with the use of subwavelength gratings [31], polarization grating axicons [32], and quantized Pancharatnam Berry phase elements in conjugation with an axicon [33]. Similarly, experimental measurements of vector vortex beams are limited, consisting of over-complicated interferometric techniques [34].

In this Letter, we present a novel yet simple procedure for the creation and detection of non-diffracting vector Bessel beams [35, 36]. A SLM and a q-plate, which converts scalar fields into cylindrical vector fields, are used to generate our vector vortex beams. We simultaneously detect both the polarization and azimuthal modes of our generated modes by implementing a PG, to separate the polarization components, and a second SLM, to consequently perform an azimuthal modal decomposition. Although this technique is tested with single-charged Bessel beams and superpositions, it can easily be extended to other OAM-carrying modes. We suggest that non-diffracting vector Bessel beams will

*adudley@csir.co.za; phone +27 (0)12 841 3741

Complex Light and Optical Forces VIII, edited by David L. Andrews, Enrique J. Galvez, Jesper Glückstad,
Proc. of SPIE Vol. 8999, 89990K · © 2014 SPIE · CCC code: 0277-786X/14/$18 · doi: 10.1117/12.2038372

prove useful in realising hyper-entanglement due to their coupling between polarization and OAM, as well as increased bandwidth in optical communication systems as they are more resilient to atmospheric turbulence [13].

2. CONCEPT AND EXPERIMENTAL SETUP

To illustrate the concept for both the generation and measurement procedures, we mathematically describe a generalized superposition of Bessel beams in terms of its azimuthal (l) and polarization components (described by making use of the standard Jones matrix notation). Initially, a scalar Bessel beam is generated whose electric field is generalized as

$$u(r,\varphi,z=0)=\sum_{l}J_{l}(k_{r}r)\exp(il\varphi)\begin{pmatrix}1\\1\end{pmatrix}, \tag{1}$$

where $J_l(.)$ is the first order Bessel function; kr is the transverse wave-vector and the matrix denotes linear polarization. To convert this scalar field into a CV field, we introduce an azimuthally-varying birefringent plate, known as a q-plate, which performs the following transformation on the azimuthal (l) and polarization components

$$\exp(il\varphi)\begin{pmatrix}1\\1\end{pmatrix}\rightarrow\exp\left(i(l+Q)\varphi\right)\begin{pmatrix}1\\-i\end{pmatrix}+\exp\left(i(l-Q)\varphi\right)\begin{pmatrix}1\\i\end{pmatrix}, \tag{2}$$

thus producing a vector Bessel beam, whose electric field is generalized as

$$u(r,\varphi)=\sum_{l}J_{l+Q}(k_{r}r)\exp\left(i(l+Q)\varphi\right)\begin{pmatrix}1\\-i\end{pmatrix}+\sum_{l}J_{l-Q}(k_{r}r)\exp\left(i(l-Q)\varphi\right)\begin{pmatrix}1\\i\end{pmatrix}. \tag{3}$$

Here Q corresponds to the azimuthal charge introduced by the q-plate ($Q = 2q$) and the matrices correspond to left- and right- circular polarization, respectively. From Eq. (3) it is evident that the mode consists of orthogonal circular polarization components, of opposite azimuthal index, thus rendering a vector vortex beam. Subsequently, a polarizer (whose transmission axis is set at an angle of θ with respects to the $+x$-axis) can be used to filter specific polarization states, resulting in the intensity profile of the field being described as

$$I(r,\varphi,\theta)=\left(\sum_{l}J_{l+Q}(k_{r}r)\right)^{2}+\left(\sum_{l}J_{l-Q}(k_{r}r)\right)^{2}+2\sum_{l}J_{l+Q}(k_{r}r)\sum_{l}J_{l-Q}(k_{r}r)\cos(2\theta+2Q\varphi). \tag{4}$$

To perform a measurement of the polarization and azimuthal components of the generated field it is evident from Eq. (3) that the field can be separated into its left- and right-circular polarization modes. These polarization modes are sorted with the use of a PG, which acts as a polarizing beam-splitter for left- and right-circular polarization. The field after the PG is

$$u(r,\varphi)=\begin{cases}\sum_{l}J_{l+Q}(k_{r}r)\exp\left(i(l+Q)\varphi\right)\\ \sum_{l}J_{l-Q}(k_{r}r)\exp\left(i(l-Q)\varphi\right)\end{cases}, \tag{5}$$

in the output ports for left- and right-circular polarization, respectively. Since any optical field can be mathematically expressed in terms of modes, constituting of orthogonal basis functions, once the modes have been sorted according to their polarization, the weightings (c_l) of their azimuthal modes are extracted by performing an azimuthal decomposition by means of an inner-product

$$c_{n}=\left\langle u,t_{n}\right\rangle=\iint ut_{n}^{*}dxdy \tag{6}$$

Here u denotes the field of interest as described in Eq. (5) and $t_n = \exp(in\varphi)$ is termed the match-filter. When the azimuthal mode index, n, of the match-filter, tn, is the complex conjugate of one of the azimuthal modes present in the field of interest, described by Eq. (5), the weighting of the azimuthal mode, c_n is non-zero. In the case that the azimuthal mode index, n, is not the complex conjugate of one of the azimuthal modes present in the field of interest, the weighting c_n is zero.

The experimental setup for generating and measuring non-diffracting vector Bessel beams is depicted in Fig. 1, highlighted by divisions 1 and 2, respectively. To generate various superimposed scalar Bessel beams, as described by

Eq. (1), an expanded HeNe laser beam (λ ~ 633 nm) was directed onto the liquid crystal display of a SLM, labelled SLM1. These fields were generated in a similar approach to Durnin's ring-slit aperture method [22], implemented digitally [37] on SLM1 (Holo-Eye, PLUTO-VIS, with 1920 x 1080 pixels of pitch 8 um and calibrated for a 2π phase shift at λ = 633 nm) with the use of complex amplitude modulation [38-40].

The beam plane of SLM1 was relay imaged (lenses L1 and L2) onto a second SLM (SLM2, same specifications as SLM1) which was used to find the weightings of the azimuthal modes by performing the inner-product measurement as described in Eq. (6). An aperture in the Fourier plane of SLM1 was used to select the first diffraction order and block all remaining ones. A q-plate, performing the transformation described in Eq. (2), was placed within the imaging system so as to convert the scalar Bessel fields into cylindrical vector Bessel fields. Since SLM1 is responsive to only horizontally-polarized modes and the q-plate requires an initial linearly-polarized mode in order to produce a superposition of opposite handed azimuthal modes ((l - Q) and (l + Q)) in orthogonal circular polarization states, a polarizer was introduced before the q-plate to rotate the horizontal polarization into linear polarization.

Before the azimuthal modes were extracted in division 2 of Fig. 1, a PG was introduced to diffract left- and right-circular polarization components into two separate ports. The PG was aligned appropriately so that the port containing the left-circular polarization modes were incident on SLM2 so as to extract their azimuthal modes. Later, the PG was adjusted to direct the right-circular polarization modes onto SLM2 for the execution of their azimuthal decomposition.

The inner-product (given in Eq. (6)) was executed experimentally by directing the modes onto the match-filter, encoded on SLM2 and viewing the Fourier transform, with the use of lens L3, on the CCD (Spiricon Beam-Gage, SP620U). The match-filter, an example of which is given in Fig. 1 (e), consists of an azimuthally-varying phase, exp($in\varphi$). For this particular example the weighting of the azimuthal mode, n = 3 (i.e., c_3), is being measured. By adjusting the azimuthally-varying phase, various azimuthal weightings in the optical modes can be measured. Similarly, SLM2 is also only responsive to horizontally-polarized modes. However, since the horizontal component is present in both left- and right-circular polarizations, we need not introduce additional polarization optics.

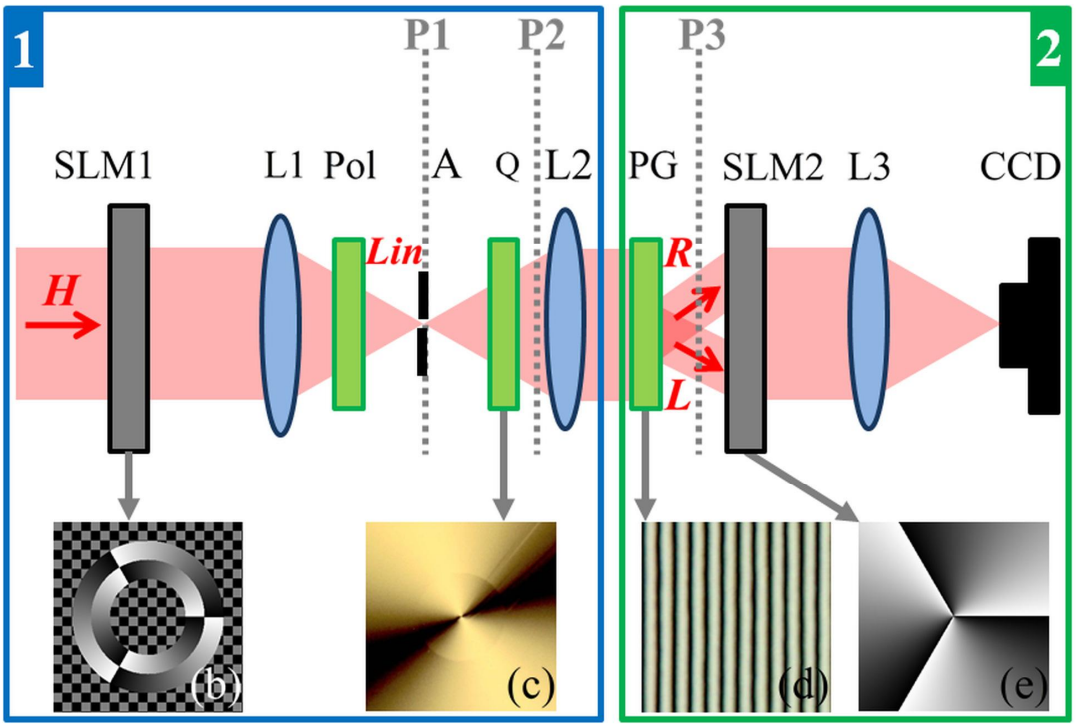

Fig. 1. (a) Schematic of the generation (division 1) and detection (division 2) of non-diffracting vector Bessel beams. SLM: spatial light modulator; L: lens (f1 and f2 = 500 mm, f3 = 300 mm); Pol: polarizer (fast axis set vertical); A: aperture; Q: q-plate; PG: polarization grating; CCD: camera. The polarization of the beam is written in red. (b) An example of a hologram used to generate a superposition of two scalar Bessel beams of azimuthal indices l = -3 and +3. Polarizing optical microscope photographs of (c) the q-plate and (d) the PG, both recorded between crossed polarizers. (e) An example of the hologram used as the match-filter to detect the azimuthal index l = +3.

3. RESULTS AND DISCUSSION

Scalar single-charged Bessel beams as well as superpositions were generated with SLM1 and an example of the near- and far-field for each is shown in the top row of Fig. 2. Figure 2 (a) ((c)) contains a scalar single-charged zero-order Bessel beam (superimposed Bessel beams of azimuthal indices l = -2 and +2), as described by Eq. (1) and recorded at plane P1 in Fig. 1 and its corresponding far-field depicted in (b) ((d)). In the case of the superposition, the azimuthal indices are of equal magnitude, but opposite handedness resulting in the predicted petal-structure, where the number of petals is denoted by $2|l|$ [37]. The fields entering the q-plate are linearly polarized (an equal weighting of left- and right-circular polarization), resulting in the left-circular component being converted to the right-circular component, while decreasing the azimuthal component by a unit charge of OAM. The reverse procedure takes place on the right-circular component, converting it to left while simultaneously increasing the azimuthal component by a unit charge of OAM. The resulting field after the q-plate is presented in Fig. 2 (e) and (g), which was recorded at plane P2 in Fig. 1 and is described by Eq. (3). This field is a non-diffracting vector Bessel beam whose polarization is radial (i.e. it consists of both left- and right-circular polarizations). In the case of the of the zero-order Bessel beam, the OAM associated with the left-circular component increases by an unit charge of OAM (while the right-circular component decreases by a unit charge of OAM) thus producing a superposition of two Bessel beams of azimuthal indices l = -1 and +1, illustrated by the 2 petals ($2|l|$) in Fig. 2 (e).

Similarly, the superimposed Bessel beams of azimuthal indices l = -2 and +2 becomes a superimposition of Bessel beams of azimuthal indices l = -3;-1 and +3 after the q-plate as illustrated in Fig. 2 (g) (l = -2 → -1 and +3, while l = +2 → -1 and -3). The corresponding far-fields of Fig. 2 (e) and (g) are given in (f) and (h). The inserts in Fig. 2 (e) and (g) display the individual left- and right-circular components recorded at plane P3 in Fig. 1 which can be described by Eq. (5). The top (bottom) insert in Fig. 2 (e) contains the left- (right-) circular component which is a Bessel beam of azimuthal index l = +1 (l = -1). Similarly, the top (bottom) insert in Fig. 2(g) contains the left- (right-) circular component which is a superposition of Bessel beams of azimuthal indices l = -3 and +3 (l = -3 and -1) denoted by the four-lobe ($l_1 + l_2$) petal structure. The corresponding far-field experimental images, for the left- and right-circular components, are given as inserts in in Fig. 2 (f) and (h). Here the number of singularities in the far-field is denoted by $2|l|$ or $l_1 + l_2$ (the same as the number of petals) [41]. The polarizer (positioned before the q-plate in Fig. 1) was rotated to illustrate that the intensity profile of the vector Bessel field rotates in agreement with Eq. (4) and can be viewed in Fig.4 of Ref. [35].

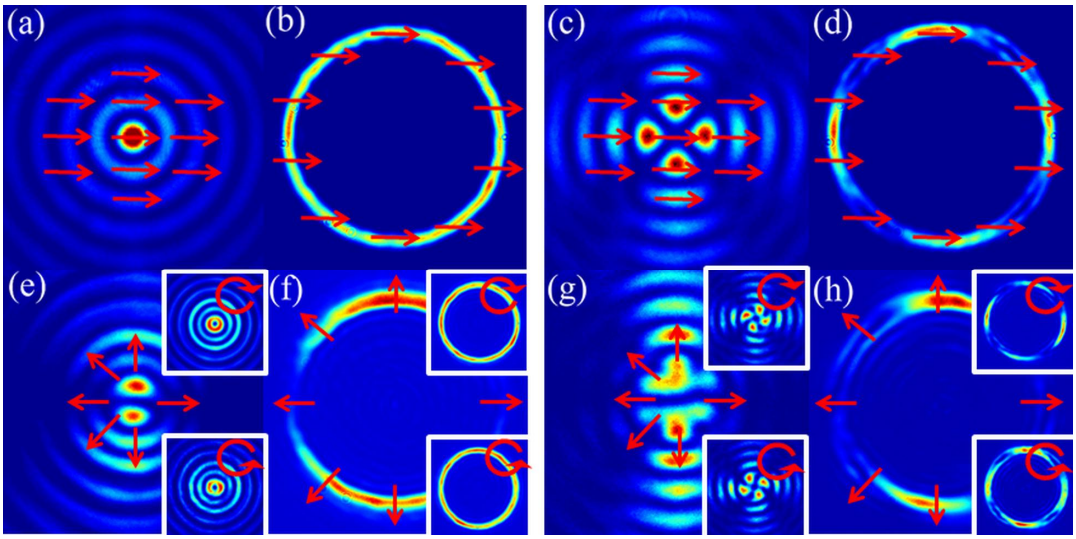

Fig. 2. Experimentally recorded (a) ((c)) near- and (b) ((d)) far-field intensity profiles of the scalar single charged Bessel beam of azimuthal index l= 0 (superimposed scalar Bessel beams of azimuthal indices l = -2 and +2). Corresponding experimental (e) ((g)) near- and (f) ((h)) far-field intensity profiles of the cylindrical vector Bessel fields recorded after the q-plate. Inserts denote the corresponding left- (top) and right-circular (bottom) polarization components. Red arrows denote the polarization direction.

An azimuthal decomposition was performed on each polarization component of the generated non-diffracting vector single-charged Bessel beams and the results are depicted in Fig 3 (blue) and (green) for the left- and right-circular components, respectively. The measurement of the azimuthal indices, presented in Fig. 3 (blue) ((green)), illustrates that

the scalar single-charged Bessel beams incur an increase (decrease) in their OAM when passing through the q-plate given by the diagonal occurring below (above) the centre diagonal, marked by the red dotted line, as expected from the transformation in Eq. (2).

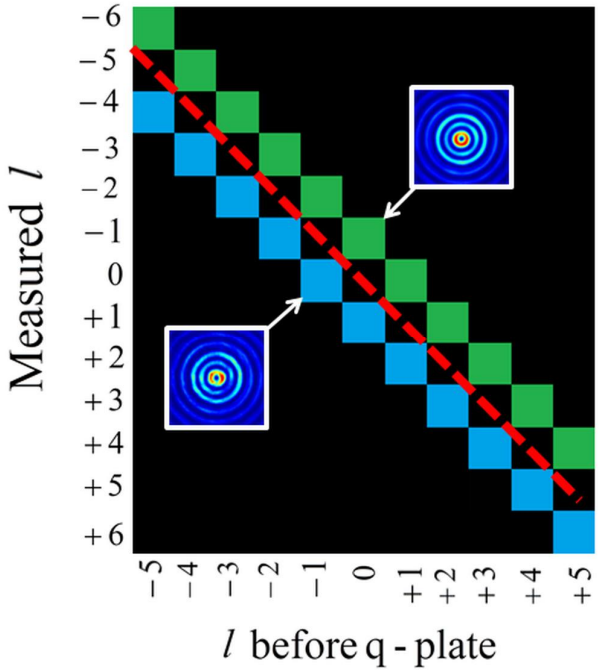

Fig. 3. Relative fractions of the correlation signals for match-filters ranging from l = -6 to +6 for initial scalar single-charged Bessel beams ranging from l = -5 to +5 for both the (blue) left- and (green) right-circular polarization components. Inserts: l = 1 and l = -1 Bessel beams after the q-plate associated with left- and right-circular polarization components, respectively.

4. CONCLUSION

In conclusion, we have shown an experimental realisation of non-diffracting vector Bessel beams with a simple method that requires only two optical elements: a SLM for the creation of the scalar fields and a q-plate for the conversion into cylindrical vector vortex fields. We detected the polarization of the generated field with the use of a PG, as well as their azimuthal modes by performing an azimuthal modal decomposition with a second SLM and a Fourier transforming lens. We were able to extract the azimuthal modes present in the non-diffracting vector Bessel beams with high accuracy and in good agreement with theory. Having the ability to simultaneously control both the polarization and OAM degrees of freedom will prove useful in hyper-entanglement systems, especially those that would benefit from the non-diffracting and self-reconstructing properties of Bessel beams as in the case of long-range communication.

REFERENCES

[1] Zhan, Q., "Cylindrical vector beams: from mathematical concepts to applications," Adv. Opt. Photon 1, 1 (2009).

[2] Brown, T. G. and Zhan, Q., "Introduction: Unconventional Polarization States of Light Focus Issue," Opt. Express 18, 10775 (2010).

[3] Hasman, E., Biener, G., Niv, A. and Kleiner, V., [Space-variant polarization manipulation], Elsevier, 215-289 (2005).

[4] Brown, T. G., [Unconventional polarization states: beam propagation, focusing and imaging], Elsevier, 8-129 (2011).

[5] Beckley, A. M., Brown, T. G., and Alonso, M. A., "Full Poincare beams,"Opt. Express 18, 10777 (2010).

[6] Pohl, D., "Operation of a Ruby laser in the purely transverse electric mode TE01," Appl. Phys. Lett. 20, 266 (1972).

[7] Mushiake, Y., Matzumurra, K., and Nakajima, N., "Generation of radially polarized optical beam mode by laser oscillation," Proc. IEEE 60, 1107 (1972).
[8] Grosjean, T., Courjon, D., and Spajer, M., "An all-fiber device for generating radially and other polarized light beams," Opt. Commun 203, 1 (2002).
[9] Dai, J. and Zhan, Q., "Beam shaping with vectorial vortex beams under low numerical aperture illumination condition," Proc SPIE, Vol. 7062 (2008).
[10] Han, W., Cheng, W., and Zhan, Q., "Flattop focusing with full Poincare beams under low numerical aperture illumination," Opt. Lett. 36, 1605 (2011).
[11] Dorn, R., Quabis, S., and Leuchs, G., "Sharper focus for a radially polarized light beam," Phys. Rev. Lett. 91, 233901 (2003).
[12] Roxworthy, B. J. and Toussaint, K. C., "Optical trapping with pi-phase cylindrical vector beams," New J. Phys. 12, 073012 (2010).
[13] Cheng, W., Haus, J. W., and Zhan, Q., "Propagation of vector vortex beams through a turbulent atmosphere," Opt. Express 17, 17829 (2009).
[14] Soskin, M. S. and Vasnetsov, M. V., [Singular optics], Elsevier, 219-276 (2001).
[15] Nye, J. F., "Polarization effect in the diffraction of electromagnetic waves: the role of disclinations," Proc. R. Soc. Lond. A 387, 105 (1983).
[16] Nye, J. F., "Lines of circular polarization in electromagnetic wave fields," Proc. R. Soc. Lond. Ser. A 389, 279 (1983).
[17] Hajnal, J. V., "Singularities in the transverse fields of electromagnetic waves," Proc. R. Soc. Lond. A 414, 433 (1987).
[18] Freund, I., "Polarization singularity indices in Gaussian laser beams," Opt. Commun. 201, 251 (2002).
[19] Dennis, M. R., "Polarization singularities in paraxial vector fields: morphology and statistics," Opt. Commun. 213, 201 (2002).
[20] Beijersbergen, M. W., Allen, L., Van der Veen, H. E. L. O., and Woerdman, J. P., "Astigmatic laser mode converters and the transferof orbital angular momentum," Opt. Commun. 96, 123 (1993).
[21] Allen, L., Beijersbergen, M. W., Spreeuw, R. J. C., and Woerdman, J. P., "Orbital angular momentum of light and the transformation of Laguerre-Gaussian laser modes," Phys. Rev. A 45, 8185 (1992).
[22] Durnin, J., Miceli Jr., J.J., and Eberly, J. H., "Diffraction-free beams," Phys. Rev. Lett. 58, 1499 (1987).
[23] Turunen, J., Vasara, A., and Friberg, A. T., "Holographic generation of diffraction-free beams," Appl. Opt. 27, 3959 (1988).
[24] Vasara, A., Turunen, J., and Friberg, A. T., "Realization of general nondiffracting beams with computer-generated holograms," J. Opt. Soc. Am. A 6, 1748 (1989).
[25] Indebetouw, G., "Nondiffracting optical fields: some remarks on their analysis and synthesis," J. Opt. Soc. Am. A 6, 150 (1989).
[26] Garces-Chavez, V., McGloin, D., Melville, H., Sibbett, W., and Dholakia, K., "Simultaneous micromanipulation in multiple planes using a self-reconstructing light beam," Nature 419, 145 (2002).
[27] McLaren, M., Agnew, M., Leach, J., Roux, F. S., Padgett, M. J. , Boyd, R. W., and Forbes, A., "Entangled Bessel-Gaussian beams," Opt. Express 20, 23589 (2012).
[28] MacDonald, R. P., and Boothroyd, S. A., and Okamoto, T., and Chrostowski, J., and Syrett, B. A., "Interboard optical data distribution by Bessel beam shadowing," Opt. Commun. 122, 169 (1996).
[29] Bouchal, Z., Wagner, J., and Chlup, M., "Self-reconstruction of a distorted nondiffracting beam," Opt. Commun. 151, 207 (1998).
[30] Litvin, I., McLaren, M., and Forbes, A., "A conical wave approach to calculating Bessel-Gauss beam reconstruction after complex obstacles" Opt. Commun. 282, 6 (2009).
[31] Bomzon, Z., and Niv, A., and Biener, G., and Kleiner, V., and Hasman, E., "Non-diffracting periodically space-variant polarization beams with subwavelength gratings," Appl. Phys. Lett. 80, 3685 (2002).
[32] Tervo, J., and Turunen, J., "Generation of vectorial propagation-invariant fields by polarization-grating axicons," Opt. Commun. 192, 13 (2001).
[33] Niv, A., Biener, G., Kleiner, V., and Hasman, E., "Propagation-invariant vectorial Bessel beams obtained by use of quantized Pancharatnam-Berry phase optical elements," Opt. Lett. 29, 238 (2004).
[34] Milione, G., and Evans, S., and Nolan, D. A., and Alfano, R. R., "Higher Order Pancharatnam-Berry Phase and the Angular Momentum of Light," Phys. Rev. Lett. 108, 190401 (2012).

[35] Dudley, A., Li, Y., Mhlanga, T., Escuti, M., and Forbes, A., "Generating and measuring nondiffracting vector Bessel beams," Opt. Lett. 38(17), 3429-3432 (2013).
[36] Li, Y., Dudley, A., Mhlanga, T., Escuti, M., and Forbes, A., "Generating and analyzing non-diffracting vector vortex beams," Proc. SPIE 8843 (2013).
[37] Vasilyeu, R., and Dudley, A., and Khilo, N., and Forbes, A., "Generating superpositions of higher-order Bessel beams," Opt. Express 17, 23389 (2009).
[38] Wong, D. W. K., and Chen, G., "Redistribution of the zero order by the use of a phase checkerboard pattern in computer generated holograms," Appl. Opt. 47, 602 (2008).
[39] Lopez-Mariscal, C., and Helmerson, K., "Shaped nondiffracting beams," Opt. Lett. 35, 1215 (2010).
[40] Dudley, A., and Vasilyeu, R., and Belyi, V., and Khilo, N., and Ropot, P., and Forbes, A., "Controlling the evolution of nondiffracting speckle by complex amplitude modulation on a phase-only spatial light modulator," Opt. Commun. 285, 5 (2012).
[41] Dudley, A., and Forbes, A., "From stationary annular rings to rotating Bessel beams," J. Opt. Soc. Am. A 29, 567 (2012).